Water Practice & Technology

IWA PUBLISHING

Water Practice & Technology Vol 17 No 1, 1 doi: 10.2166/wpt.2021.089

Improving the ZnO-photocatalytic degradation of humic acid using powdered residuals from water purification plant

Mohamed Elmougi[a,*], Hisham El-Etriby[a], Ragab Barakat[a], Mohamed Gar Alalm[a,b] and Mohamed Mossad[a]

[a] Department of Public Works Engineering, Faculty of Engineering, Mansoura University, Mansoura 35516, Egypt
[b] Department of Chemical Engineering, Polytechnique Montreal, C.P. 6079, Montreal H3C 3A7, Quebec, Canada
*Corresponding author. E-mail: mohamed.m.elmougi@gmail.com

ABSTRACT

Alum residuals were collected from a water treatment plant and used for improving the photocatalytic degradation of humic acid (HA) by combinations of zinc oxide (ZnO) and powdered residuals from a water purification plant (PRWPP). The influence of operating conditions such as initial humic acid concentration, pH, irradiation time, PRWPP to ZnO ratio, catalyst dose, and light illuminance have been investigated. The optimum PRWPP to ZnO ratio was 10:90. Using the prepared composites instead of bare ZnO raised the HA removal efficiency from 85.5% to 97.8%, and from 38% to 48.1% at catalyst doses of 1.2 g/l and 0.4 g/l, respectively. Moreover, it reduced energy consumption from 210.4 to 166.2 Wh per mg of HA. An artificial neural network model (ANN) was developed to predict the removal efficiency under different operating conditions. The optimum ANN structure yielded a coefficient of determination ($R^2 = 0.993$). A modified Langmuir-Hinshelwood pseudo-first-order model was used for describing the degradation kinetics at different initial concentrations of HA.

Key words: alum, humic acid, photocatalysis, residuals, ZnO

HIGHLIGHTS

- Adding PRWPP enhanced the removal efficiency, reduced the ZnO dosage, and reduced the energy consumption.
- PRWPP addition had a positive outcome on the environment, and its impact was confirmed using an ANN model.
- HA photocatalytic degradation was found to be dependent on catalyst dosage, initial HA concentration, pH, retention time, and light illuminance.

GRAPHICAL ABSTRACT

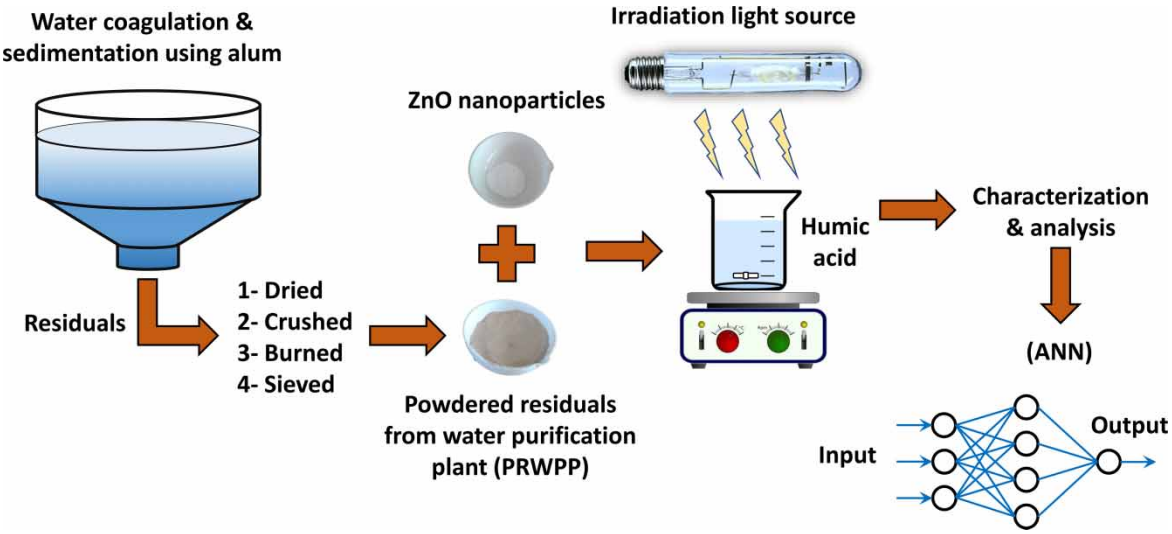

INTRODUCTION

Coagulation followed by flocculation, sedimentation, and filtration is considered the conventional, most used technique in water treatment plants worldwide (Dassanayake *et al.* 2015). In this process, a chemical coagulant, mostly aluminum salts, is added to help destabilize the electrical double-layered colloids and reduce the repulsive forces between the colloid particles; as a result, colloids agglomerate to form flocs and settle easily (Matilainen *et al.* 2010). This process is associated with producing large amounts of residuals, most of which are considered as waste and are disposed of into sewerage systems or landfills (Dassanayake *et al.* 2015). The increasing financial and environmental costs require alternative solutions such as sludge reuse or recycling. Numerous studies have been carried out to see the possibility of using the sludge, including but not limited to, using sludge as adsorbents in water and wastewater treatment processes (Gibbons & Gagnon 2011), as a coagulant aid (Jangkorn *et al.* 2011), and as an enhancement to the electrocoagulation process (Khedher *et al.* 2017).

Humic substances are dark brown, structurally complex, and polyelectrolytic materials that represent the major percentage of natural organic matter (NOM). They comprise 40–80% of the dissolved organic carbon in natural waters. They are generated from the microbial degradation of dying plants and animals (Uyguner *et al.* 2007). Humic substances can be subcategorized according to solubility properties into three main groups: humic acid (HA), which is soluble in water at $pH > 2$; fulvic acid (FA), which is soluble in water at all pH conditions; and humin that is insoluble in water at any pH level (Uyguner *et al.* 2007). NOM is a major concern in water treatment for its ability to react with residual chlorine forming disinfection by-products (DBPs), such as trihalomethanes and haloacetic acids (Richardson *et al.* 2007). These DBPs have detrimental effects on human health when humans are exposed to them via dermal contact, ingestion or inhalation. The US Environmental Protection Agency (USEPA) regulates the maximum concentration of DBPs in safe drinking water at levels of 80 μg/l and 60 μg/l for trihalomethanes and haloacetic acids, respectively (U.S. Environmental Protection Agency 2006). Several approaches have been employed to remove humic acid or NOM, such as conventional or advanced coagulation, membrane filtration, ion exchange, adsorption using activated carbon, and advanced oxidation processes (AOPs) like ozonation, photo-Fenton, and heterogeneous photocatalysis (Liu *et al.* 2008).

AOPs in general and photocatalysis in particular stand out compared to other processes as they work by forming hydroxyl radicals (˙OH) that can achieve unselective mineralization of organic matter instead of turning them into another phase, which could cause secondary pollution, and require regular disposal and/or treatment (Patsios *et al.* 2013). In addition, NOM removal using conventional treatment processes has been linked with several problems. For instance, coagulation, which is considered the most used technique for NOM removal, can partially remove NOM and a portion of NOM still remains in the final water, especially the low molar mass and hydrophilic part of the NOM, even by using advanced coagulation (Matilainen *et al.* 2010). Nanofiltration, another highly effective technique for NOM removal, was found to cause significant membrane fouling (Gowland *et al.* 2021). These problems contributed to increasing the number of research projects dedicated towards alternative techniques like photocatalysis. Photocatalysis process can be performed by irradiating a semi-conductor catalyst, typically titanium dioxide (TiO_2) or to lesser extent zinc oxide (ZnO), using a light source with energy higher than the band gap energy of the catalyst to form hydroxyl radicals (˙OH) that can oxidize different types of contaminants (Gerrity *et al.* 2009). ZnO photocatalysis was reported to achieve up to 98.95% of HA removal after a two-stage process at an initial humic acid concentration of 10 mg/L, pH 4.0, ZnO dosage of 0.5 g/l and a retention time of 30 min (Oskoei *et al.* 2016).

The aim of this study is to investigate the possibility of adding powdered residuals from a water purification plant (PRWPP) as an enhancement to the ZnO-photocatalysis process for HA degradation. This addition is intended to reduce the ZnO dosage, minimize the energy consumption, and decrease the process cost. The study also aims to develop an ANN model for predicting the removal efficiency at different operating conditions using the experimental results.

MATERIALS AND METHODS

Chemicals and materials

HA and ZnO nanoparticles were purchased from Alfa Aesar, Germany, to be used as the main contaminant, and the photo-catalyst, respectively. The obtained ZnO nanoparticles had specific surface area of 12 m^2/g, and average particle size of 67 nm. A stock solution of humic acid was prepared by dissolving 100 mg of humic acid into

1,000 mL of distilled water using a magnetic stirrer. The stock solution was then stored in a refrigerator for later use.

Preparation of PRWPP

Water treatment residuals were obtained from the Galya water treatment plant in Dakahlia, Egypt, where alum is used as the main coagulant in the coagulation process. The residuals were collected from the dewatering tank in solid form. They were crushed into fine particles, dried at 105 °C for 24 hours, burned at 500 °C for 3 hours, and passed through No. 200 sieve to maintain a particle size less than 75 μm (Khedher *et al.* 2017).

Characterization of PRWPP

The chemical composition of the PRWPP was determined by energy dispersive X-ray spectroscopy (EDS) using a scanning electron microscope (Jeol JSM-6510LV). The structure shape of the PRWPP was investigated using a scanning electron microscope (SEM). The Fourier transform infrared spectroscopy (FTIR) was performed using an FTIR spectrometer (Thermo Scientific Nicolet IS10) to identify the existing chemical bonds in the studied material.

Bench-scale photocatalytic system

The photocatalytic system consisted of a 250 ml Pyrex beaker as the batch reactor filled with HA solution at the desired concentration and placed 11 centimeters below a 400-Watt metal halide lamp (Phillips) with a maximum wavelength of 510 nm, and photon flux of 220 μW cm^{-2}. The beaker was placed on a magnetic stirrer to keep the catalyst in suspension. The whole system was set up inside a wooden container.

Experimental conditions

ZnO photocatalysis processes were performed at initial humic acid concentrations of 5, 10, 15, 20, and 25 mg/l; ZnO nanoparticles dosages of 0.4, 0.6, 0.8, 1, and 1.2 g/l; and pH levels of 3,5,7,9, and 11. First, the degradation studies were done using standard ZnO photocatalysis, then the PRWPP were added at 5, 10, and 20% of the total (ZnO + PRWPP) dosage. All experiments were carried out at room temperature using a sample volume of 300 ml for a contact time of 255 min divided into two phases; the first 15 min were in darkness, while the remaining 240 min were under light irradiation. All experiments were performed three times and the final presented results were calculated as the mean value of all three.

Sampling and analysis

10 ml samples were drawn after the first 15 min, then every 30 min afterward. The samples were kept motionless for 60 min for settling of nanoparticles. Then, the samples were centrifuged for 30 min at speed of 4,000 rpm using a centrifuge (MLW-T54, Germany) to settle the remaining particles.

The concentration of HA was determined using a spectrophotometer (AG Lab, N4S, 200–1,000 nm, USA) at wavelength 254 nm (UV_{254}). The removal ratio of humic acid (R%) was determined from Equation (1):

$$R\% = \frac{C_0 - C}{C_0} \times 100 \tag{1}$$

where C_0 is the initial humic acid concentration, while C is the humic acid concentration at retention time (t).

The energy consumed in Watt-hours per milligram of humic acid removed (E/HA), and the amount of humic acid removed in milligrams per gram of added ZnO nanoparticles (HA/ZnO) were also determined using Equations (2) and (3) respectively:

$$E/HA = \frac{P\,t}{R\,C_0\,V} \tag{2}$$

$$HA/ZnO = \frac{R\,C_0}{Z} \tag{3}$$

where P is the power of the light source in Watts, t is the time in hr, R is the humic acid removal ratio, C_0 is the initial humic acid concentration in mg/l, V is the water volume in liters, and Z is the ZnO dosage in g/l.

Artificial neural network (ANN) model

An artificial neural network (ANN) model was developed using MATLAB software to simulate the influence of operating conditions on the removal efficiency of HA. The model is of feed-forward back propagation type and is comprised of an input layer, a hidden layer, and an output layer. The input layer includes six neurons to represent initial concentration, pH, catalyst dose, PRWPP/ZnO ratio, irradiation time, and light illuminance. The output layer is composed of neuron representing the removal efficiency of HA. The optimum number of the neurons in the hidden layer is investigated to obtain a network structure with the least mean square error (MSE).

RESULTS AND DISCUSSION

Characterization of PRWPP

Figure 1 shows the EDS spectrum of all constituents of the PRWPP. The sample was coated with gold (Au), which explains its presence in the EDS spectrum. The detailed chemical composition in Table 1 shows that the main elements of the PRWPP were O, C, Al, Si, Fe, Cu, Zn, Ca, Mg, and K. The SEM image in Figure 2 shows that PRWPP have no regular form or shape with numerous pores on the outer surface that could increase the contact chances with water pollutants.

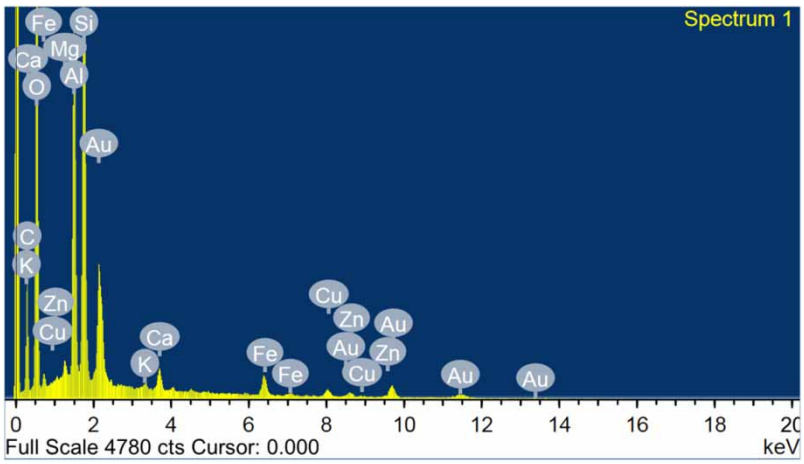

Figure 1 | EDS spectrum of the PRWPP.

Table 1 | Chemical composition of the PRWPP

Composition	O	C	Si	Al	Fe	Cu	Zn	Ca	Mg	K
Amount (wt.%)	49.45	28.48	9.36	7.5	1.74	1.2	0.96	0.73	0.39	0.19

The FTIR spectrum is plotted in Figure 3. It shows several absorption bands between 4,000 cm^{-1} and 3,000 cm^{-1}. The wide band at 3,447 cm^{-1} is attributed to the stretching vibration of O–H, while the band located at 1,630 cm^{-1} is associated with the bending vibration of water molecules O–H–O chemically associated with aluminum hydroxide $Al(OH)_3$ (Ahmad *et al.* 2016). Hydrocarbon chains of the organic materials in the sludge can be detected at the bands between 3,000 cm^{-1} and 2,800 cm^{-1}; however, the 2,931 cm^{-1} band represents the asymmetrical stretching vibration of C–H from methylene groups (De Oliveira Silva *et al.* 2012). Absorption band located at 1,475 cm^{-1} is related to stretching vibration of C–O in carbonate. Both bands at 1,080 cm^{-1} and 796 cm^{-1} are attributed to stretching vibration in quartz Si–O–Si, while bending vibration of O–Si–O can be detected at 469 cm^{-1} (Ahmad *et al.* 2016). Band recorded at 675 cm^{-1} is attributed to stretching vibration of Al-O (Khedher *et al.* 2017). Table 2 lists the summary of all major absorption peaks and the assigned functional groups corresponding to their wavenumbers. According to FTIR spectrum, the PRWPP consisted of hydrocarbons and different oxides like silica and aluminum oxide, as well as aluminum hydroxide.

Effect of PRWPP to ZnO ratio

A set of experiments were conducted to compare the usage of ZnO only, PRWPP only, or both ZnO and PRWPP together as the catalyst in the photocatalytic reaction at different PRWPP percentages (5, 10, and 20%). The

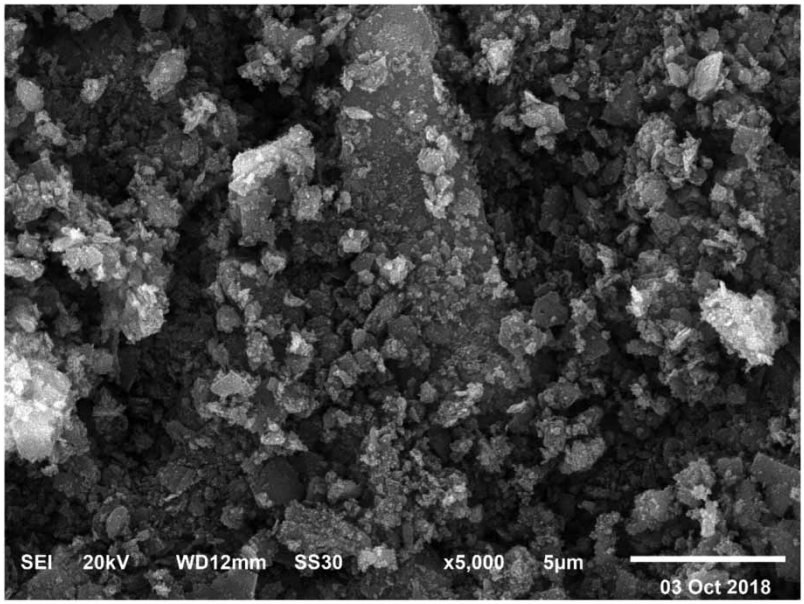

Figure 2 | SEM image of the PRWPP.

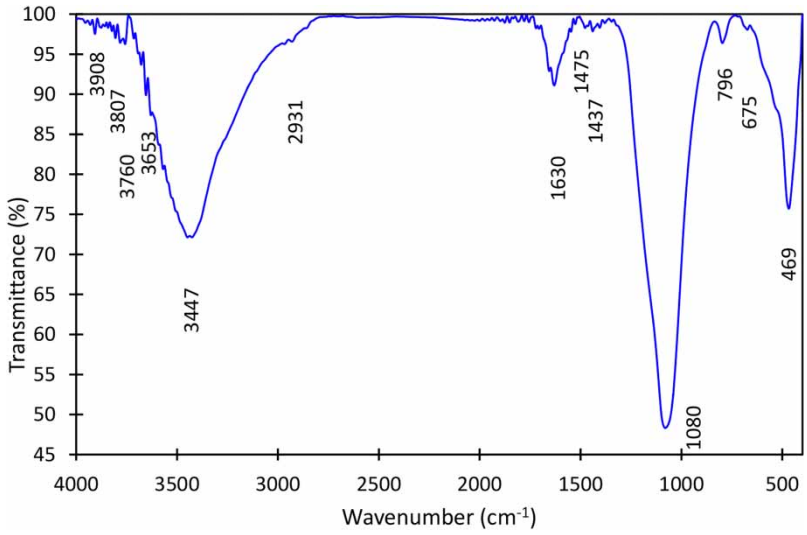

Figure 3 | FTIR spectrum of the PRWPP.

Table 2 | Functional groups and the corresponding wavenumbers in the FTIR spectrum

Wavenumber cm^{-1}	Assignment
3,447	Stretching vibration of (O–H)
2,931	Asymmetrical stretching vibration of (C–H)
1,630	Bending vibration of (H–O–H)
1,475	Stretching vibration of (C–O)
1,080 & 796	Stretching vibration of (Si–O–Si)
675	Stretching vibration of (Al–O)
469	Bending vibration of (O–Si–O)

experiments were performed at an initial HA concentration of 25 mg/l, pH value of 7.0, and (ZnO + PRWPP) dose of 1.2 g/l.

Firstly, using PRWPP separately achieved 46.7% HA removal after the first 15 minutes without light irradiation. However, with the light source on, the removal efficiency gained insignificant increase from 46.7% to 56.5% after 105 min of retention time (Figure 4(a)). The phenomenon indicates that PRWPP does not acquire photocatalytic properties and despite its adsorptive affinity towards HA, the removal efficiency did not go beyond 56.5%. Thus, PRWPP adsorption alone is insufficient to completely remove HA from water. When PRWPP was added to ZnO nanoparticles, the removal efficiency increased from 85.53% (using ZnO alone) to 97.85%, 95.98%, and 92.77% using 10, 20, and 5% PRWPP of the added catalyst, respectively (Figure 4(a)). This improvement could be attributed to the high adsorption ability of the PRWPP towards HA because of its amorphous nature, which helps trap HA particles inside the pores available on its surface. Additionally, aluminum hydroxide, which is a main component of alum-coagulation residuals, showed high affinity towards HA more than any other type of NOM (Bose & Reckhow 1998). Aluminum hydroxide is relatively insoluble in water especially in the pH range of 5–7; thus, at low mixing speed the particles start precipitating, removing any particulate that gets enmeshed in them (Tchobanoglous *et al.* 2004). Moreover, Figure 4(a) shows that the PRWPP addition enhanced the removal ratio at the end of the first 15-minute-dark phase, thus reducing the remaining HA concentration in the second phase, and increasing the free sites on the ZnO surface.

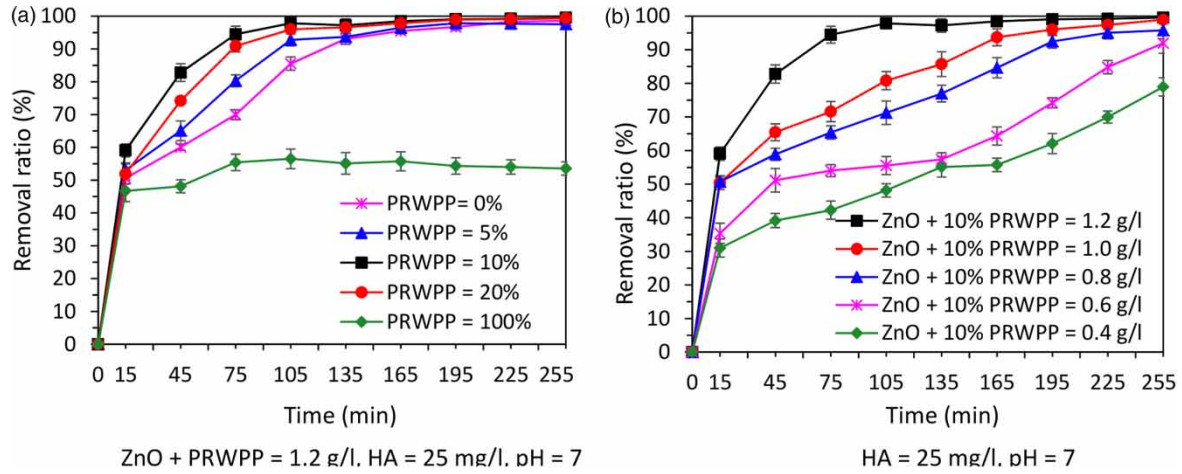

Figure 4 | HA removal efficiency at (a) different PRWPP ratio, and (b) different ZnO + PRWPP dosages.

On the other hand, increasing PRWPP percentage from 10% to 20% decreased the removal efficiency from 97.85% to 95.98% at retention time of 105 minutes. It could be due to the fact that at 20% PRWPP, the amount of ZnO was decreased from 90% to 80% of the total (PRWPP + ZnO) catalyst, which resulted in less free sites on the catalyst surface. In addition, increasing the PRWPP concentration resulted in higher water turbidity that prevented the UV light flux from reaching the active sites of ZnO nanoparticles. Therefore, the PRWPP to catalyst ratio was maintained at 10% for all the later experiments.

Effect of (ZnO + PRWPP) dose on humic acid removal ratio

Different (ZnO + PRWPP) doses of 0.4, 0.6, 0.8, 1.0, and 1.2 g/l were added with PRWPP to catalyst ratio of 10% and initial humic acid concentration of 25 mg/l. It was found that increasing the dose led to higher HA removal efficiencies. Figure 4(b) shows that after 105 min, the removal efficiencies were 48.1%, 55.5%, 71.2%, 80.8%, and 97.8% at catalyst doses of 0.4, 0.6, 0.8, 1.0, and 1.2 g/l, respectively. This phenomenon may be attributed to the increasing number of adsorbent active sites at higher doses, which can capture more humic acid molecules and lead to a higher removal efficiency (Oskoei *et al.* 2016). However, increasing the adsorbent dosage decreased its adsorption uptake (the amount of humic acid adsorbed per gram of the added adsorbent) (Figure 5(a)).

Effect of PRWPP addition on energy consumption and ZnO amount

The addition of PRWPP in the photocatalytic process did not only enhance the degradation of HA but also decreased the required amount of ZnO and reduced energy consumption. Batch studies were carried out first without adding PRWPP, then by adding PRWPP at initial humic acid concentration of 25 mg/l, pH 7.0, lamp's

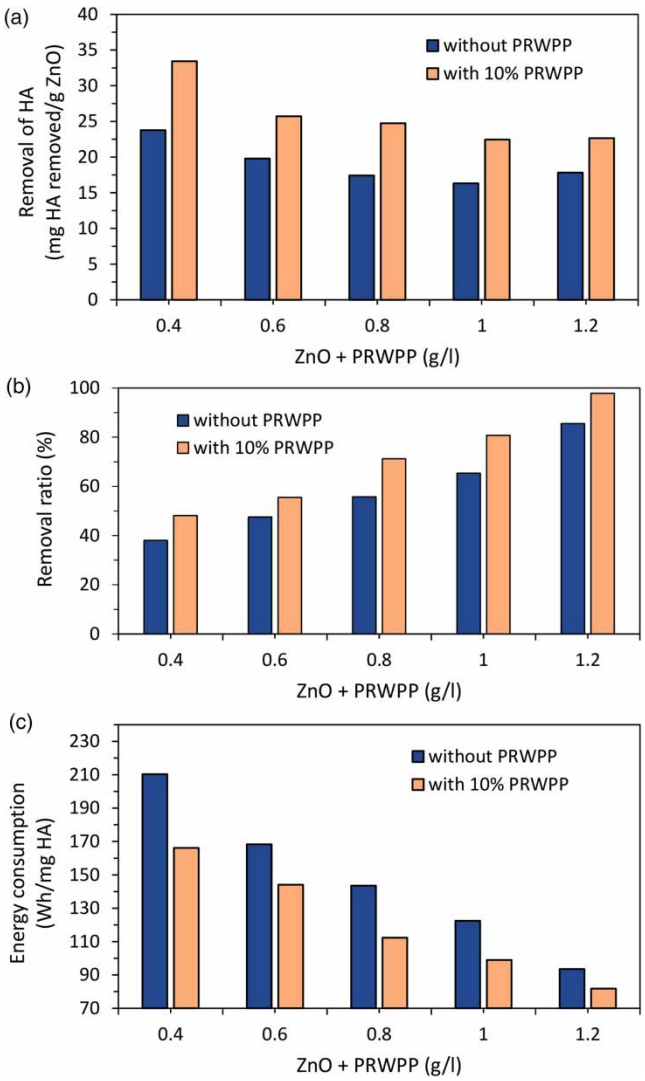

Figure 5 | Comparison between HA photocatalytic degradation with and without PRWPP. (a) Removal of HA (mg HA removed/g ZnO added), (b) HA removal efficiency, and (c) energy consumption per amount of HA removed in Wh/mg HA. (Condition: Retention time = 105 min, HA = 25 mg/l, pH = 7, and power = 400 W).

power of 400 W, and retention time of 105 min. Figure 5(b) shows that adding PRWPP increased the HA removal efficiency at all the ZnO doses. Adding 10% PRWPP of the catalyst dose of 0.4 g/l increased the removal ratio from 38% to 48.1%, which is very close to the removal ratio at ZnO-only dosage of 0.6 g/l. As a result, the amount of ZnO required was saved by 0.2 g/l.

The amount of humic acid removed per one gram of ZnO nanoparticles was calculated using Equation (3), and the results are shown in Figure 5(a). The results indicate that adding PRWPP improved the ZnO removal capacity by 40.6% at catalyst dosage of 0.4 g/l. Figure 5(c) depicts the energy consumed in Watt-hours per milligram of humic acid removed, which was calculated by Equation (2). It shows that adding PRWPP saved 26.6% of the energy consumed to reach the required removal efficiency at ZnO + PRWPP = 0.4 g/l. It is clear that increasing the amount of added PRWPP decreased the energy consumed per milligrams of humic acid removed.

Effect of pH on humic acid removal ratio

Different pH levels of 3, 5, 7, 9, and 11 were tested to investigate the pH influence on HA removal efficiency at an initial concentration of 25 mg/l, ZnO + 10% PRWPP dose of 0.4 g/l, and retention time of 255 minutes. Figure 6(a) shows that at lower pH levels, the removal efficiencies were higher and vice versa. This phenomenon can be attributed to the fact that ZnO tends to have a positive charge at pH lower than its point of zero charge (PZC), which lies in the pH range of 8.7–9 (Kosmulski 2006), which increases its ability to electrostatically adsorb

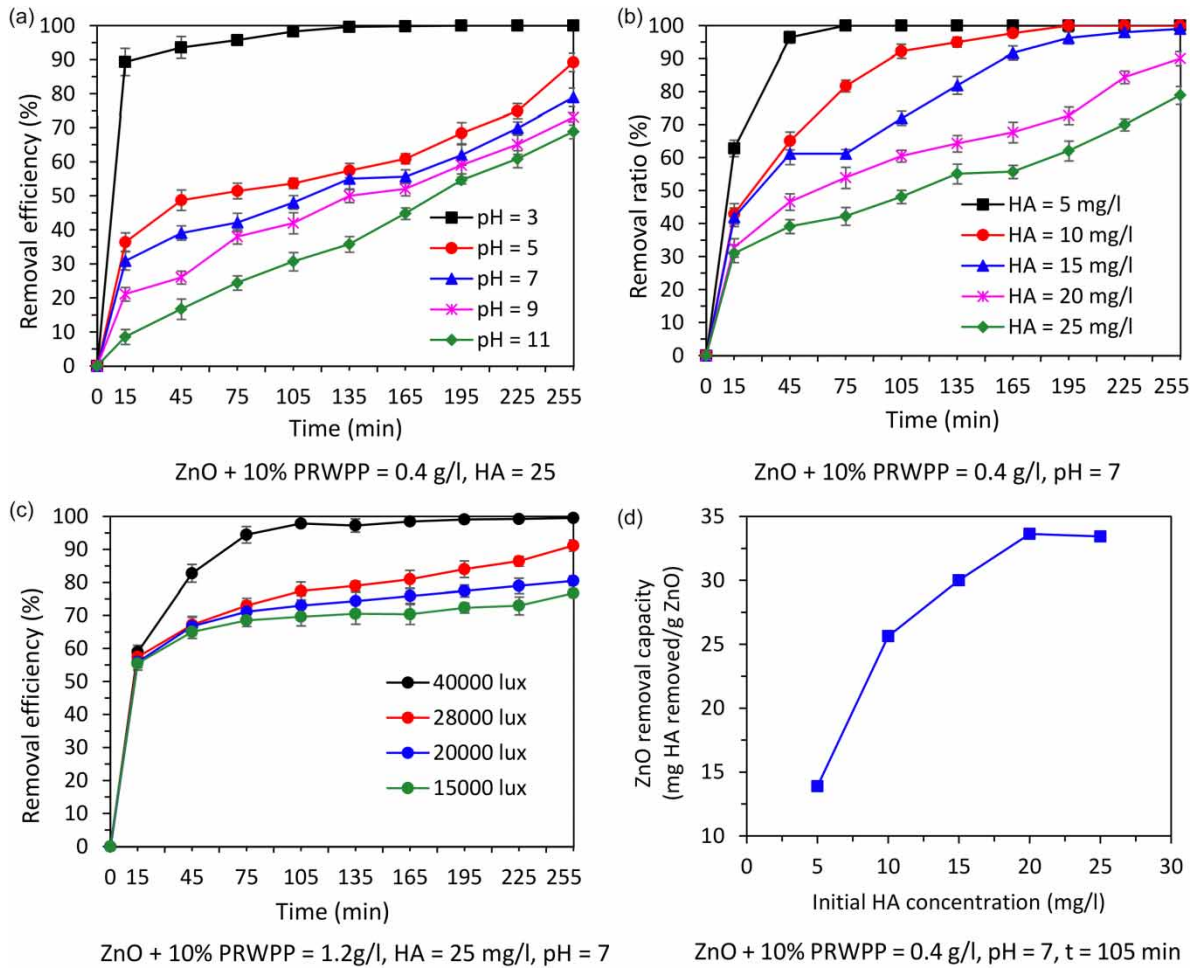

Figure 6 | HA removal efficiency at (a) different pH levels, (b) different initial HA concentrations, and (c) different light illuminance; (d) shows the effect of initial HA concentration on ZnO adsorption capacity.

humic acid anions, while ZnO usually has negative charge at pH higher than PZC, thus repelling negatively-charged HA particles (Chong *et al.* 2010; Oskoei *et al.* 2016). In addition, the acidic environment provides H^+ ions leading to more $^{\bullet}H$ radicals that can react with oxygen to form hydroperoxyl radicals HO_2, which eventually produce hydroxyl radicals $^{\bullet}OH$ (Oskoei *et al.* 2016).

Effect of initial humic acid concentration on the removal ratio

Different initial humic acid concentrations (5, 10, 15, 20, and 25 mg/l) were tested to study the influence of initial HA concentration. The experiments were conducted using ZnO + 10% PRWPP of 0.4 g/l, a pH level of 7, and total retention time of 255 minutes. The results showed an inverse proportion between initial humic acid concentration and the final removal efficiency as depicted in Figure 6(b). This could be explained by the fact that ZnO + PRWPP doses were fixed for all the reactors; hence the same amount of $^{\bullet}OH$ radicals was produced in each one. Decreasing HA concentration provided more free sites on the adsorbent surface and more free $^{\bullet}OH$ radicals for oxidation reactions, which led to higher removal efficiencies. Increasing the humic acid concentration beyond 20 mg/l reduced the removal capacity of ZnO for humic acid, as shown in Figure 6(d). This reduction was due to the repulsive forces between the negatively-charged molecules, which resulted in lower adsorption on the catalyst surface (Oskoei *et al.* 2016).

Effect of light illuminance

In order to study the influence of light illuminance on humic acid removal efficiency, the beaker was placed at different distances apart from the light source. Distances of 11, 21, 31, and 41 cm between the top of the beaker and the light source resulted in light illuminance values of 40,000, 28,000, 20,000, and 15,000 lux, respectively. It is clear from Figure 6(c) that decreasing the light illuminance decreased the removal efficiency from 99.5% at

40,000 lux to 91.2%, 80.5%, and 76.7% at 28,000, 20,000, and 15,000 lux, respectively by the end of the contact time. This finding can be explained by the fact that increasing the distance between the beaker and the lamp decreased the number of photons reaching the solution and irradiating ZnO nanoparticles, thus producing fewer hydroxyl radicals, thereby causing lower removal efficiencies.

Artificial neural network (ANN) model

A series of ANN models were trained using a different number of neurons in the hidden layer, which varied between 4 and 16 neurons. The maximum allowed number of epochs (iterations) for the training of all models was 1,000. The transfer function employed in the hidden layer was the hyperbolic tangent sigmoid function (tansig). The input data was weighted through the links between neurons, and then the obtained weights were stored in a bias between the input and hidden layers. The transfer functions in the hidden layer generated activations using the weighted data that have been obtained in the previous step. The activations were weighted by the connections between the hidden and output neurons, then the weights were stored in a bias. The value of the removal efficiency (Output neuron) was then determined by the transfer function. The errors between the actual and the determined values were calculated, then all the weights were recalculated in a backpropagation process. All the previous steps are defined as one epoch. The epochs were repeated many times until the desired mean square error (MSE) was attained. The MSE was calculated as an error function according to Equation (4):

$$MSE = \frac{1}{N}\sum_{i=1}^{i=Q}(y_{i.\mathrm{pred}} - y_{i.\mathrm{exp}})^2 \tag{4}$$

where N is the number of data points, $y_{i.\mathrm{pred}}$ is the ANN predicted value, $y_{i.\mathrm{exp}}$ is the experimental value, and i is the point number. The highest correlation and lowest MSE were attained by a model with one hidden layer containing 10 neurons, so the final ANN structure is (6–10–1) as shown in Figure 7(a). The R^2 of the training, validation, and testing are 0.9923, 0.9953, and 0.9956, while the overall R^2 is 0.9932, as shown in Figure 8. The final weights were used to determine the relative importance for all the operational conditions affecting the removal efficiency. The relative importance of all inputs was calculated based on the partitioning of connection weights employing Equation (5) (Radwan *et al.* 2018):

$$I_J = \frac{\sum_{m-1}^{m-N_h}\left(\left(|\overset{ih}{W}_{jm}|/\sum_{k-1}^{N_i}|\overset{ih}{W}_{km}|\right)\times|\overset{ho}{W}_{mn}|\right)}{\sum_{k-1}^{k-N_i}\left\{\sum_{m-1}^{m-N_h}\left(|\overset{ih}{W}_{km}|/\sum_{k-1}^{N_i}|\overset{ih}{W}_{km}|\right)\times|\overset{ho}{W}_{mn}|\right\}} \tag{5}$$

where I_J is the relative importance of the j^{th} input. N_i and N_h refer to the numbers of the input and the hidden neuron, respectively. W represents the connection weights determined by the training of the ANN. The superscripts 'i', 'h' and 'o' represent the input, the hidden and the output layers, respectively. The subscripts 'k', 'm' and 'n' refer to the input, the hidden and the output neurons, respectively. Figure 7(b) depicts the relative importance of each parameter. The results showed that all the considered parameters have strong influences on the removal efficiency, and thus, none of the elements was excluded from the optimized ANN model. Moreover, the PRWPP/ZnO ratio showed the highest relative importance, which confirms the effective role of PRWPP in the mechanism of HA degradation.

Kinetics of humic acid degradation

The kinetics of humic acid photocatalytic degradation were investigated using a modified Langmuir–Hinshelwood model as expressed in Equation (6) since it was proved to be appropriate for fitting the degradation kinetics of different contaminants by photocatalysis in previous literature (Narayana *et al.* 2011; Gar Alalm *et al.* 2018).

$$r = -\frac{dC}{dt} = \frac{k_r k_{ad} C}{1 + k_{ad} C} \tag{6}$$

where k_r is the reaction rate constant, k_{ad} is the equilibrium constant for adsorption, and C is the humic acid concentration. At lower concentrations of HA, the integrated form of Equation (6) can be simplified into a pseudo-first-

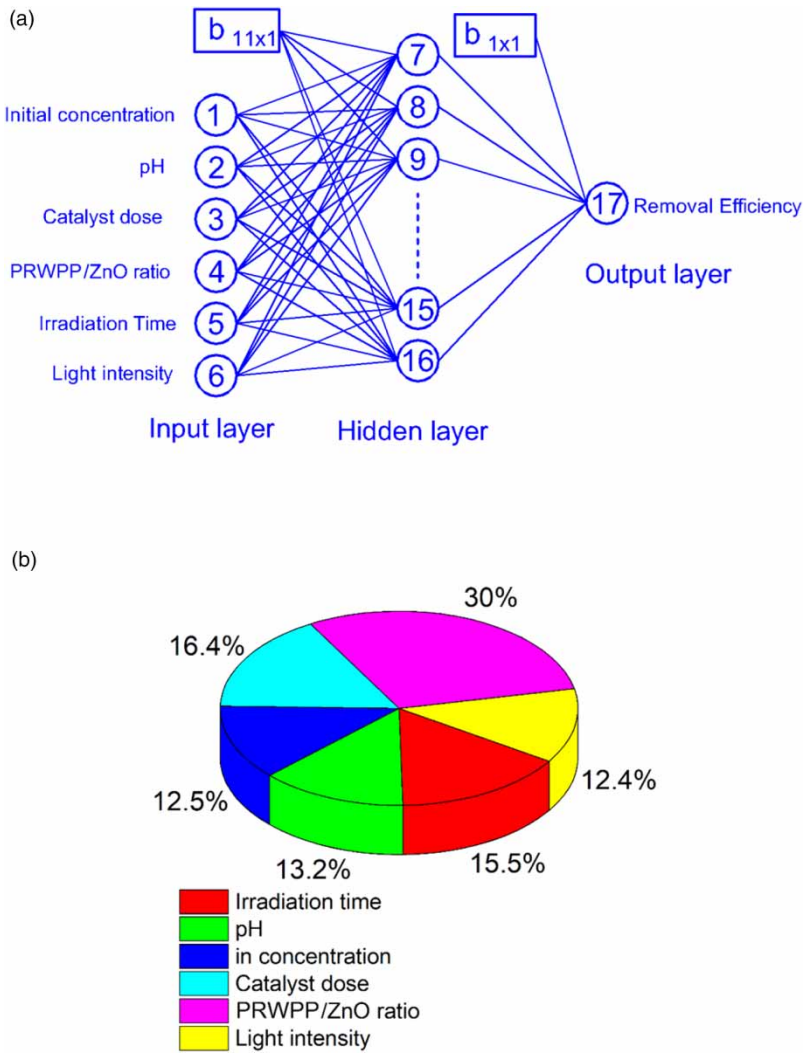

Figure 7 | (a) The structure of the ANN model, and (b) the relative importance of the ANN inputs.

order form, as shown in Equation (7) (Gar Alalm *et al.* 2018).

$$\ln\left(\frac{C_0}{C}\right) = k_r k_{ad} t = k_{app} t \tag{7}$$

where C_0 is the initial humic acid concentration, k_{app} is the apparent pseudo-first-order rate constant, and t is the retention time. Figure 9 depicts the pseudo-first-order relation between $\ln(C_0/C)$ and time at different initial humic acid concentrations, and their k_{app} and R^2 are listed in Table 3. The results show high correlation with Langmuir–Hinshelwood model with $R^2 = 0.911$–0.998 at initial humic acid concentrations ($C_0 = 5$–20 mg/l).

CONCLUSION

In this study, the addition of powdered alum residuals to ZnO nanoparticles for improving the photocatalytic degradation of HA was investigated. It was found that the removal efficiency was affected by different parameters, such as PRWPP dose, catalyst dose, initial humic acid concentration, pH, retention time, and light illuminance. The highest degradation efficiency was attained using a combination of PRWPP and ZnO ratio of 10:90. The optimum pH for the degradation of HA was 3.0. Decreasing the initial HA concentration led to higher removal efficiencies, while decreasing ZnO + PRWPP dose, retention time, or light illuminance decreased the removal efficiency. The PRWPP addition led to an improvement of the removal efficiency by 15.5%. In addition, it increased the removal capacity of ZnO by 40.6% and decreased energy consumption by 26.6%. An artificial

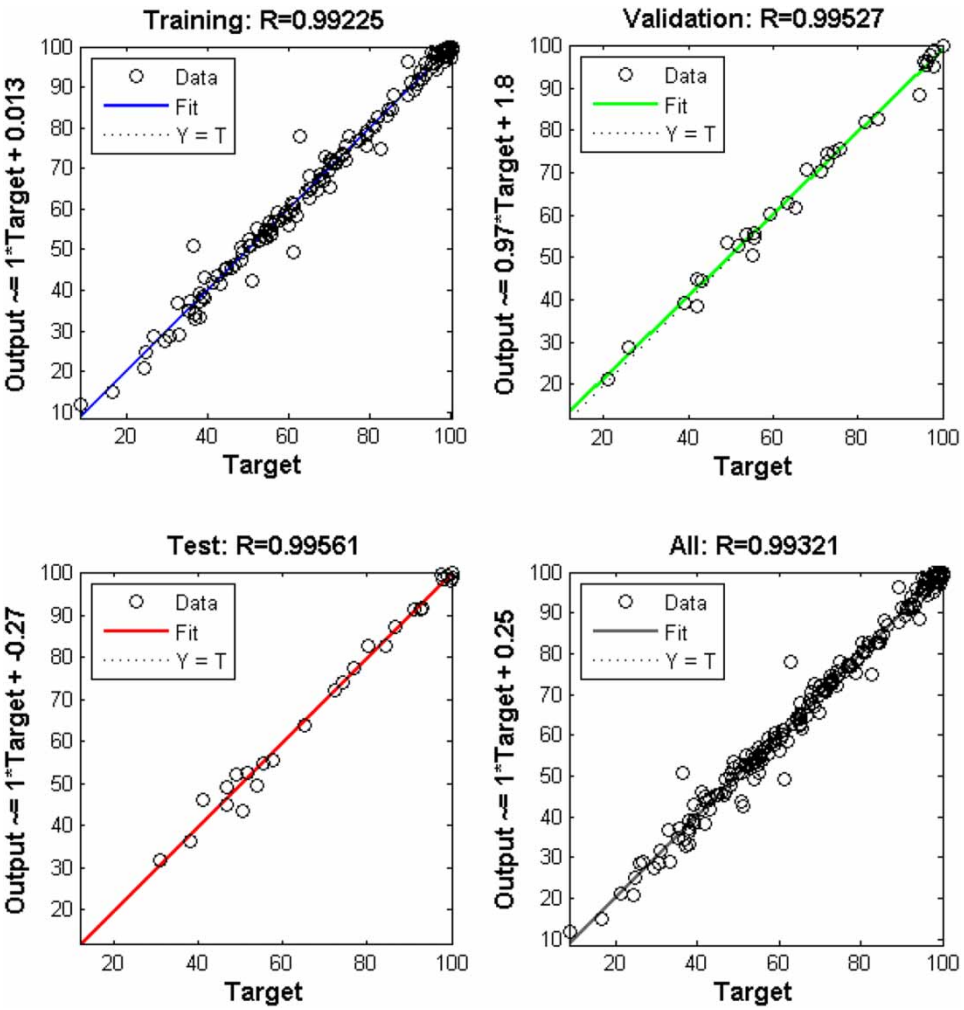

Figure 8 | The correlation between the ANN output and target data.

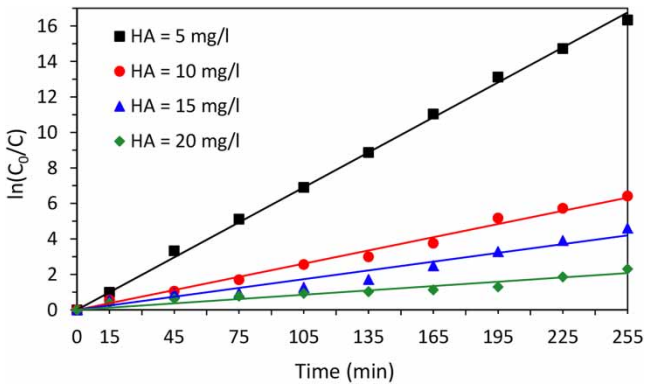

Figure 9 | Kinetics of humic acid degradation at different initial humic acid concentrations (ZnO + 10% PRWPP = 0.4 g/l, pH = 7).

Table 3 | Analysis of the Langmuir-Hinshelwood model

Initial concentration (mg/l)	k_{app}	R^2
5	0.0657	0.998
10	0.0248	0.99
15	0.0165	0.956
20	0.0081	0.911

neural network model (ANN) was developed and the calculated relative importance of its input parameters confirmed the importance of PRWPP addition. The modified Langmuir–Hinshelwood model was found to be suitable for describing the humic acid degradation kinetics. Overall, the application of residuals along with ZnO was found to be effective for removal of HA. It will be beneficial for the environment as the consumption of sludge will decrease its loading into landfills. Using enhanced photocatalysis instead of traditional photocatalysis could increase the process' applicability in large-scale water and wastewater treatment plants. The current commercial use of photocatalysis in the water industry has been limited to smaller-scale systems, mainly because of its high energy consumption and high cost. Enhanced photocatalysis reduced the process' energy consumption and reduced its cost, which is a huge step towards the promising future of photocatalysis applications in water treatment.

DATA AVAILABILITY STATEMENT

All relevant data are included in the paper or its Supplementary Information.

REFERENCES

Ahmad, T., Ahmad, K., Ahad, A. & Alam, M. 2016 Characterization of water treatment sludge and its reuse as coagulant. *Journal of Environmental Management* **182**, 606–611.

Bose, P. & Reckhow, D. A. 1998 Adsorption of natural organic matter on preformed aluminum hydroxide flocs. *Journal of Environmental Engineering* **124**(9), 803–811.

Chong, M. N., Jin, B., Chow, C. W. K. & Saint, C. 2010 Recent developments in photocatalytic water treatment technology: a review. *Water Research* **44**(10), 2997–3027.

Dassanayake, K. B., Jayasinghe, G. Y., Surapaneni, A. & Hetherington, C. 2015 A review on alum sludge reuse with special reference to agricultural applications and future challenges. *Waste Management* **38**, 321–335.

De Oliveira Silva, J., Filho, G. R., Da Silva Meireles, C., Ribeiro, S. D., Vieira, J. G., Da Silva, C. V. & Cerqueira, D. A. 2012 Thermal analysis and FTIR studies of sewage sludge produced in treatment plants. The case of sludge in the city of Uberlândia-MG, Brazil. *Thermochimica Acta* **528**, 72–75.

Gar Alalm, M., Samy, M., Ookawara, S. & Ohno, T. 2018 Immobilization of S-TiO_2 on reusable aluminum plates by polysiloxane for photocatalytic degradation of 2,4-dichlorophenol in water. *Journal of Water Process Engineering* **26**, 329–335.

Gerrity, D., Mayer, B., Ryu, H., Crittenden, J. & Abbaszadegan, M. 2009 A comparison of pilot-scale photocatalysis and enhanced coagulation for disinfection byproduct mitigation. *Water Research* **43**(6), 1597–1610.

Gibbons, M. K. & Gagnon, G. A. 2011 Understanding removal of phosphate or arsenate onto water treatment residual solids. *Journal of Hazardous Materials* **186**(2), 1916–1923.

Gowland, D. C. A., Robertson, N. & Chatzisymeon, E. 2021 Photocatalytic oxidation of natural organic matter in water. **13**(3), 288.

Jangkorn, S., Kuhakaew, S., Theantanoo, S., Klinla-or, H. & Sriwiriyarat, T. 2011 Evaluation of reusing alum sludge for the coagulation of industrial wastewater containing mixed anionic surfactants. *Journal of Environmental Sciences* **23**(4), 587–594.

Khedher, M., Mossad, M. & El-Etriby, H. K. 2017 Enhancement of electrocoagulation process for dye removal using powdered residuals from water purification plants (PRWPP). *Water, Air, and Soil Pollution* **228**(8), 293.

Kosmulski, M. 2006 pH-dependent surface charging and points of zero charge: III. Update. *Journal of Colloid and Interface Science* **298**(2), 730–741.

Liu, S., Lim, M., Fabris, R., Chow, C., Drikas, M. & Amal, R. 2008 TiO_2 photocatalysis of natural organic matter in surface water: impact on trihalomethane and haloacetic acid formation potential. *Environmental Science & Technology* **42**(16), 6218–6223.

Matilainen, A., Vepsäläinen, M. & Sillanpää, M. 2010 Natural organic matter removal by coagulation during drinking water treatment: a review. *Advances in Colloid and Interface Science* **159**(2), 189–197.

Narayana, R. L., Matheswaran, M., Aziz, A. A. & Saravanan, P. 2011 Photocatalytic decolourization of basic Green dye by pure and Fe, Co doped TiO_2 under daylight illumination. *Desalination* **269**(1), 249–253.

Oskoei, V., Dehghani, M. H., Nazmara, S., Heibati, B., Asif, M., Tyagi, I., Agarwal, S. & Gupta, V. K. 2016 Removal of humic acid from aqueous solution using UV/ZnO nano-photocatalysis and adsorption. *Journal of Molecular Liquids* **213**, 374–380.

Patsios, S. I., Sarasidis, V. C. & Karabelas, A. J. 2013 A hybrid photocatalysis–ultrafiltration continuous process for humic acids degradation. *Separation and Purification Technology* **104**, 333–341.

Radwan, M., Gar Alalm, M. & Eletriby, H. 2018 Optimization and modeling of electro-Fenton process for treatment of phenolic wastewater using nickel and sacrificial stainless steel anodes. *Journal of Water Process Engineering* **22**, 155–162.

Richardson, S. D., Plewa, M. J., Wagner, E. D., Schoeny, R. & DeMarini, D. M. 2007 Occurrence, genotoxicity, and carcinogenicity of regulated and emerging disinfection by-products in drinking water: a review and roadmap for research. *Mutation Research/Reviews in Mutation Research* **636**(1), 178–242.

Tchobanoglous, G., Burton, F. L. & Stensel, H. D. 2004 Fundamentals of chemical coagulation. In: *Metcalf & Eddy Wastewater Engineering: Treatment and Reuse* (Tchobanoglous, G., Burton, F. L. & Stensel, H. D., eds). McGraw-Hill Inc., New York, NY, pp. 478–493.

U.S. Environmental Protection Agency 2006 National primary drinking water regulations: stage 2 disinfectants and disinfection byproducts rule: final rule. *USEPA Federal Register* **71**(2), 387–493.

Uyguner, C. S., Bekbolet, M. & Swietlik, J. 2007 Natural organic matter: definitions and characterization. In: *Advances in Control of Disinfection by-Products* (Nikolau, A., Rizzo, L. & Selcuk, H., eds). Nova Publishers, Hauppauge, New York, NY, pp. 5.1–5.25.

First received 4 December 2020; accepted in revised form 3 September 2021. Available online 16 September 2021